

# Postselection-free entanglement dynamics via spacetime duality

Matteo Ippoliti<sup>1</sup> and Vedika Khemani<sup>1</sup>

<sup>1</sup>*Department of Physics, Stanford University, Stanford, CA 94305, USA*

The dynamics of entanglement in ‘hybrid’ non-unitary circuits (for example, involving both unitary gates and quantum measurements) has recently become an object of intense study. A major hurdle toward experimentally realizing this physics is the need to apply *postselection* on random measurement outcomes in order to repeatedly prepare a given output state, resulting in an exponential overhead. We propose a method to sidestep this issue in a wide class of non-unitary circuits by taking advantage of *spacetime duality*. This method maps the purification dynamics of a mixed state under non-unitary evolution onto a particular correlation function in an associated unitary circuit. This translates to an operational protocol which could be straightforwardly implemented on a digital quantum simulator. We discuss the signatures of different entanglement phases, and demonstrate examples via numerical simulations. With minor modifications, the proposed protocol allows measurement of the purity of arbitrary subsystems, which could shed light on the properties of the quantum error correcting code formed by the mixed phase in this class of hybrid dynamics.

The dynamics of quantum entanglement is a topical area of research in several subfields of physics ranging from quantum information and quantum gravity to condensed matter and atomic physics [1–13]. In a closed quantum system undergoing unitary time-evolution, thermalization of local observables is understood via the growth of entanglement between different subsystems—as recently demonstrated in beautiful experiments on Bose-Hubbard systems [14, 15] and trapped ions [16, 17]. In another recent development, various works have studied entanglement dynamics in *non-unitary* settings in which the system of interest is repeatedly subject to local measurements [18–41] and, instead of averaging over measurement outcomes, one considers the dynamics of individual quantum trajectories [42] corresponding to particular sequences of measurement outcomes. Such “monitored dynamics” are an essential feature of near-term quantum devices in which modulated interactions with an environment, say via measurements, are necessary for unitary control and feedback.

From the point of view of many-body physics, the questions of interest pertain to the types of universal dynamics one can obtain in monitored settings. Towards this end, recent works have shown that the steady states of monitored unitary-measurement (or measurement-only) circuits can display a variety of novel entanglement phases and phase transitions [18–41]. For example, individual quantum trajectories in unitary circuits interspersed with projective measurements can transition from being volume-law to area-law entangled as the measurement rate is increased; the volume-law phase is understood as a type of quantum error correcting code (QECC) in which quantum information is “hidden” from the decohering effects of local measurements [21, 22]. The properties of the measurement-induced entanglement phase transition and of the steady-state phases themselves – especially the nature of the QECC in the volume law phase [30, 38, 39] – are active areas of study.

Measuring entanglement generally requires the prepara-

ration of many identical copies of the same state (either simultaneously or sequentially) [43–49]. In the presence of measurements, this becomes extremely challenging as it requires *postselection*: a quantum measurement is an intrinsically random process whose outcomes are sampled stochastically with Born probabilities, and a quantum trajectory in this evolution is associated with a *specific* record of measurement outcomes. Hence, preparing multiple copies of the same state incurs a postselection overhead that is exponential in the number of measurements made, and thus in the size  $L$  and depth  $T$  of the circuit,  $e^{O(pLT)}$  (assuming a finite measurement rate  $p$ ). There are ways to partly overcome this challenge: (i) using a single reference qubit as a *local probe* of the entanglement phase [23], which considerably alleviates the postselection overhead; (ii) in Clifford circuits, using a combination of classical simulations and feedback to force specific measurement outcomes by error-correcting any “wrong” ones. Nevertheless, it is still desirable to *directly* access the entanglement properties of more general non-unitary and non-Clifford evolutions.

In this Letter, we propose a novel method to access quantum entanglement in a broad class of non-unitary circuits *without* incurring an exponential postselection barrier. Specifically, we will consider non-unitary circuits that are *spacetime dual* (explained below) to unitary evolutions; and we propose a method for measuring the purity  $\text{Tr}(\rho^2)$ , which is related to the second Renyi entropy via  $\text{Tr}(\rho^2) = e^{-S_2(\rho)}$ , for the system as a whole as well as for arbitrary subsystems. This allows access to the purification dynamics of an initially mixed state, which is intimately related to the entanglement dynamics of pure states [22]. In particular, the volume-law entangled phase maps onto the *mixed* phase in which the dynamics generates a QECC that protects information from measurements, so that an initially mixed state remains mixed for exponentially long times. Subsystem purity measurements contain key information about the nature of this as-of-yet poorly understood QECC [22, 30, 39].

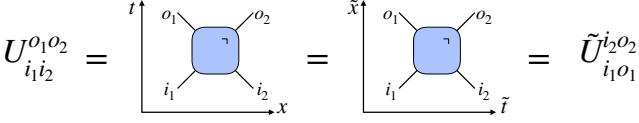


FIG. 1. Spacetime duality. By swapping the spatial and temporal axes, a unitary gate  $U$  maps onto another, generally non-unitary gate  $\tilde{U}$ .

We note that while the class of non-unitary circuits for which our method applies is not completely general, it still encompasses a vast space—as large as the space of unitary circuits built from local two-qubit gates. In particular it applies to circuits with (a specific class of) unitary gates interspersed with (specific types of) forced projective measurements.

*Spacetime duality.* Given a two-qubit unitary gate  $U_{i_1, i_2}^{o_1, o_2}$ , mapping input qubits  $i_{1,2}$  (bottom legs) to output qubits  $o_{1,2}$  (top legs), we define its spacetime dual  $\tilde{U}$  as the matrix obtained by flipping the arrow of time by 90 degrees, i.e. viewing the left legs as inputs and the right legs as outputs:  $U_{i_1, i_2}^{o_1, o_2} \equiv \tilde{U}_{i_1, o_1}^{i_2, o_2}$  (Fig. 1). The result of this transformation,  $\tilde{U}$ , is generally not unitary; gates  $U$  such that  $\tilde{U}$  is also unitary are known as “dual-unitary” and have been studied intensely recently [50–55], notably providing analytical insight into many-body quantum chaos [50]. The generic non-unitarity of  $\tilde{U}$ , and the possibility that it might counter entanglement growth, has also been employed to pursue more efficient tensor network contraction schemes [56, 57], and study the complexity of shallow (2+1)-dimensional circuits [58].

In general, one has  $\tilde{U} \equiv 2VH$ , where  $V$  is unitary and  $H$  is a positive semidefinite matrix of unit norm, which can be seen as a generalized measurement (i.e. an element of a POVM set [59], see [60] for more details). As an example,  $U = \mathbb{1}$  yields  $\tilde{U} = 2|B^+\rangle\langle B^+|$ , where  $|B^+\rangle = (|00\rangle + |11\rangle)/\sqrt{2}$  is a Bell pair state. Thus the spacetime duality transformation generally maps unitary circuits to non-unitary *hybrid circuits* involving unitary gates as well as (weak or projective) measurements, up to prefactors. Crucially, the measurements are *forced*: the outcome is deterministic; no quantum randomness is involved. In the example of  $U = \mathbb{1}$ , the outcome is always  $|B^+\rangle$ . The ability to avoid postselection in our protocol stems from this observation.

*Postselection-free measurement protocol.* We consider the purification dynamics of a fully mixed state,  $\rho_{\text{in}} \propto \mathbb{1}$ , evolved by a non-unitary circuit including forced measurements,  $M$ , as shown in Fig. 2(a). The output state,  $\rho_{\text{out}} \propto MM^\dagger$ , may be partially or completely purified. We focus on non-unitary circuits  $M$  whose spacetime dual is a unitary circuit, i.e.  $M = \tilde{U}_M$  with  $U_M$  unitary. In this case, the tensor contraction defining  $\rho_{\text{out}}$  can be performed in the dual direction in which the gates are unitary and  $\rho_{\text{out}}$  lives on a time-like slice (Fig. 2(b)).

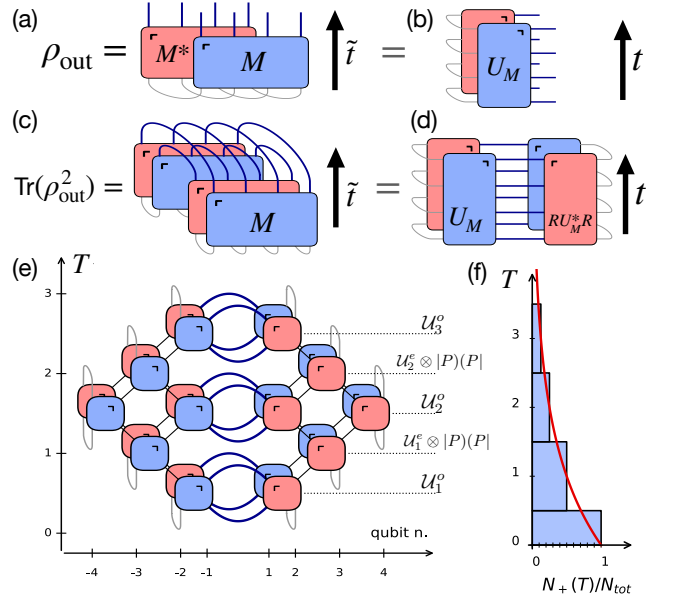


FIG. 2. (a) Purification dynamics: a fully mixed state  $\rho_{\text{in}} \propto \mathbb{1}$  (gray lines at the bottom) is evolved by a hybrid circuit  $M$  (with arrow of time  $\tilde{t}$ ), yielding a state  $\rho_{\text{out}} \propto MM^\dagger$  (blue lines at the top). (b) If  $M = \tilde{U}_M$  with  $U_M$  unitary, the purification process is ‘spacetime dual’ to a unitary evolution (with arrow of time  $t$ ).  $\rho_{\text{out}}$  lives on a time-like slice of the circuit (blue legs, right). (c) Purity of the output state,  $\text{Tr}(\rho_{\text{out}}^2)$ . (d) The purity can be interpreted as a correlation function on an associated unitary circuit. (e) Protocol for measuring the purity of  $\rho_{\text{out}}$ , sketched for  $T = 3$ . The outer tensor network legs are color-coded as in (a-d). Qubits  $\pm 1$  are repeatedly initialized in state  $P = |B^+\rangle\langle B^+|$  (upward blue arcs) and subject to Bell measurements (downward blue arcs); the protocol succeeds if all Bell measurements yield  $|B^+\rangle$ . (f) The fraction of runs that are successful up to time  $T$ ,  $N_+(T)/N_{\text{tot}}$ , equals the purity of  $\rho_{\text{out}}$  on a virtual system of  $\tilde{L} = 2T$  fully-mixed qubits evolved under hybrid dynamics for time  $\tilde{T} = T$ .

Likewise the purity,  $\text{Tr}(\rho_{\text{out}}^2)$  (Fig. 2(c)), can be interpreted as a (multi-point) correlation function in an associated unitary evolution when viewed from the dual direction, as shown in Fig. 2(d) and discussed below; this dual evolution involves a bipartite one-dimensional chain where the left half evolves under the unitary  $U_M$ , the right half evolves under the unitary  $RU_M^*R$  ( $R$  is the spatial inversion), and the only region in which the evolution is non-unitary is the central pair of qubits in the chain, which feature horizontal bonds (space-like qubit worldlines) implementing the product of  $\rho_{\text{out}}$  with itself. The goal of the following discussion is to provide an interpretation of the non-unitary processes at the central bond that allows us to convert this tensor contraction into an operational prescription for the measurement of the purity. In other words, we will use a “laboratory” system (with arrow of time  $t$ ), in which the evolution is unitary, to simulate a “dual” system (with arrow of time  $\tilde{t}$ ) in which the evolution is non-unitary and realizes

purification dynamics.

Before proceeding, let us better specify the setup. The hybrid circuit  $M$  evolves an even number  $\tilde{L}$  of qubits (we will use a tilde for quantities defined in the hybrid time evolution). The initial condition is  $\rho_{\text{in}} = \mathbb{1}/2^{\tilde{L}}$ . Unitarity of  $U_M$  in the ‘laboratory’ time direction elides all gates in the network contraction for the purity, except for those within forward and backward light cones emanating from the central non-unitary bonds; see Fig. 2(e). (This cancellation requires ‘depolarizing’ boundary conditions, which we discuss in detail in [60]). In the ‘laboratory’ (unitary) time direction, the purity calculation can be interpreted as a correlation function on a chain of  $L = \tilde{L} + 2$  qubits evolved for time  $T \equiv \tilde{L}/2$ . We symmetrically label the qubits as  $i = \{\pm 1, \pm 2, \dots, \pm (T+1)\}$ , and refer to qubits  $i \leq -2$  as  $\mathcal{L}$  (left),  $i = \pm 1$  as  $\mathcal{C}$  (central), and  $i \geq 2$  as  $\mathcal{R}$  (right).

The system is initialized in the state  $\rho \propto \mathbb{1}_{\mathcal{L}} \otimes P_{\mathcal{C}} \otimes \mathbb{1}_{\mathcal{R}}$ , where  $P = |B^+\rangle\langle B^+|$ . It is then evolved in time by a circuit with a brickwork structure. First a layer of unitary gates acts on the ‘odd’ bonds, represented by superoperator  $\mathcal{U}_t^o$ , consisting of a layer of the circuit  $U_M$  on  $\mathcal{L}$  and a layer of  $RU_M^*R$  on  $\mathcal{R}$  ( $R$  is the spatial inversion). Next, a similarly-defined layer of unitary gates  $\mathcal{U}_t^e$  acts on ‘even’ bonds, except qubits  $\pm 1 \in \mathcal{C}$ , where a *forced* Bell measurement takes place:  $\rho \mapsto P_{\mathcal{C}} \otimes \text{Tr}_{\mathcal{C}}(P_{\mathcal{C}}\rho)$ . The process terminates at time  $t = T$  with a final forced measurement of  $P_{\mathcal{C}}$ . Using the operator-state representation, in which  $|A\rangle$  denotes an operator  $A$  as a state, with inner product  $(A|B) = \text{Tr } A^\dagger B$ , we can recast the above prescription in compact form:

$$\text{Tr}(\rho_{\text{out}}^2) \propto (P|\mathcal{U}_T^o \circ \left\{ \prod_{t=1}^{T-1} [\mathcal{U}_t^e \otimes |P_{\mathcal{C}}\rangle\langle P_{\mathcal{C}}|] \circ \mathcal{U}_t^o \right\} |P), \quad (1)$$

where we use  $|P\rangle \equiv |P_{\mathcal{C}}\rangle \otimes |\mathbb{1}_{\mathcal{L} \cup \mathcal{R}}\rangle$  for compactness. The purity of the hybrid circuit output  $\rho_{\text{out}}$  is thus mapped to a  $(2T)$ -point correlation function of the projector  $P_{\mathcal{C}}$  during a unitary evolution obtained from the original hybrid circuit  $M$  via the spacetime duality.

We are now in a position to recast the result in Eq. (1) as an operational protocol for measuring the purity of the state of interest,  $\rho_{\text{out}}$ . The protocol consists of the following steps: **(1)** Choose an integer  $T$  and prepare a  $2(T+1)$ -qubit chain in the state  $\rho = \mathbb{1}_{\mathcal{L}} \otimes P_{\mathcal{C}} \otimes \mathbb{1}_{\mathcal{R}}/4^T$ . Set  $t = 1$ . **(2)** Evolve odd bonds unitarily under  $\mathcal{U}_t^o$ . **(3)** Perform a Bell measurement on  $\mathcal{C}$ . If the outcome is  $|B^+\rangle$ , continue to step 4; otherwise, stop and record a **failure**. **(4)** If  $t = T$ , stop and record a **success**; otherwise, evolve even bonds unitarily under  $\mathcal{U}_t^e$ , increment  $t$  by one, and go back to step 2.

Let the number of successful runs out of  $N_{\text{tot}}$  trials be  $N_+(T)$ ; then,

$$\text{Tr}(\rho_{\text{out}}^2|_{\tilde{L}=2T, \tilde{T}=T}) = N_+(T)/N_{\text{tot}}, \quad (2)$$

where  $\rho_{\text{out}}|_{\tilde{L}=2T, \tilde{T}=T}$  denotes the output state of hybrid dynamics on a ‘dual’ system of  $\tilde{L} = 2T$  qubits evolved for time  $\tilde{T} = T$ . This is the central result of this Letter. Note that while we have not kept track of numerical prefactors in this derivation, the proportionality constant in Eq. (2) turns out to be exactly one, see [60].

We emphasize that the above protocol, despite featuring projective measurements and runs ending in ‘failure’, does *not* use postselection. Indeed, ‘failures’ still contribute to incrementing the total number of runs  $N_{\text{tot}}$ , which enters Eq. (2) and provides crucial information for the purity measurement. In other words, copies of the same state  $\rho_{\text{out}}$  (identical up to control errors) can be realized deterministically arbitrarily many times. The exponential overhead of postselection is entirely removed.

Finally we remark that if one wants to prepare  $\rho_{\text{out}}$  in real space (as opposed to the time-like slice of the circuit obtained above), this can be achieved with an approach based on gate teleportation [59], using  $2T$  ancillas initialized in  $|B^+\rangle$  Bell states and  $O(T^2)$  SWAP gates in a 1D geometry, see [60].

*Entanglement phases.* While a typical hybrid circuit is generally *not* dual to a unitary circuit, the space of models we address is still very large, and it is reasonable to expect a rich variety of purification phases and entanglement phenomena within this class of models. Here we begin to explore this space for the purpose of demonstrating that interesting purification phases are indeed possible, and leave the longer-term enterprise of charting this space to future work.

Surprisingly, despite the presence of measurements, Eq. (2) suggests that the generic outcome of the purification dynamics in these models should be a mixed phase, in which  $\rho_{\text{out}}$  has extensive entropy. Indeed, if the late-time probability of obtaining  $|B^+\rangle$  as the outcome of the Bell measurement on  $\mathcal{C}$  approaches any value  $p_\infty < 1$ , then  $N_+(T)$ —which requires the outcome of *all*  $T$  Bell measurements to be  $|B^+\rangle$ —decays exponentially at late times. Therefore the state has a finite entropy density  $s_2$  directly measurable from a decay time constant:

$$\text{Tr}(\rho_{\text{out}}^2|_{\tilde{L}=2T, \tilde{T}=T}) \sim e^{-T/\tau} \implies s_2 \equiv (2\tau)^{-1}. \quad (3)$$

This is another main result of this Letter.

The mixed-phase outcome should be expected whenever the unitary circuit  $U_M$  features any amount of scrambling: then, any projector  $|B^+\rangle\langle B^+|$  injected in  $\mathcal{C}$  will irreversibly grow into a global operator, never refocusing at  $\mathcal{C}$ ; thus the probability of later obtaining  $|B^+\rangle$  as a Bell measurement outcome will be lower than 1, and the above argument will give a mixed phase. However, exceptions are possible in non-scrambling circuits.

As an illustration, we map out the purification phases for a specific model. For computational simplicity and closer comparison with the known phenomenology, we choose a set of unitary Clifford circuits whose space-

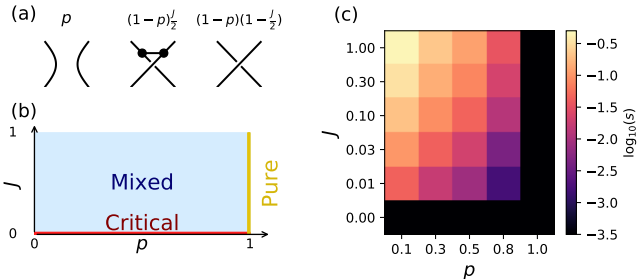


FIG. 3. (a) Summary of the Clifford circuit model: probabilities of  $\mathbb{1}$ , iSWAP and SWAP gates. (b) Schematic of purification phase diagram of the dualized circuit vs  $p$ ,  $J$ . (c) Numerically obtained entropy density of hybrid circuit output state  $\rho_{\text{out}}$  vs  $p$ ,  $J$ .

time duals consist only of unitary gates and projective Pauli measurements. We consider a brickwork layer of two-qubit Clifford gates chosen as indicated in Fig. 3(a):  $\text{Prob}(\mathbb{1}) = p$ ,  $\text{Prob}(\text{iSWAP}) = (1-p)J/2$  [61],  $\text{Prob}(\text{SWAP}) = (1-p)(1-J/2)$ . Arbitrary single-qubit Clifford gates act before and after each two-qubit gate so there are no symmetries in the model. As SWAP and iSWAP are dual-unitary while  $\tilde{\mathbb{1}} \propto |B^+\rangle\langle B^+|$  is a projector,  $p \in [0, 1]$  serves as the measurement rate for the dual hybrid circuit.  $J \in [0, 1]$  serves as an interaction rate, with  $J = 0$  giving a non-interacting ‘swap circuit’. We note that the spacetime dual of this unitary model is not too different from the original unitary-projective model considered in Ref. [18]: single-site  $Z$  measurements are replaced by two-qubit Bell measurements; gates are sampled out of exactly half of the two-qubit Clifford group, rather than the whole group. Remarkably, these seemingly small changes yield a completely different phase diagram, sketched in Fig. 3(b).

Via Clifford numerical simulations we find three possible outcomes across the  $(p, J)$  parameter space (results for the entropy density are shown in Fig. 3(c)). A pure phase is only possible at  $p = 1$ , where the circuit  $U_M$  consists purely of identity gates and  $\rho_{\text{out}} = (|B^+\rangle\langle B^+|)^{\otimes T}$  is trivially a pure state. This is unstable to infinitesimal perturbations away from  $p = 1$  (which is very unusual and counterintuitive, compared to the phase diagrams of other unitary-projective models where the pure phase is generic for sufficiently high measurement rates). For any  $J > 0$  and  $p < 1$  (i.e. almost all of parameter space) we have a mixed phase: indeed, this is the default outcome for generic interacting circuits. Finally, on the  $J = 0$  (and  $0 < p < 1$ ) line, we have a critical purification phase, with vanishing entropy density  $s_2 = 0$  but divergent entropy  $S_2 \sim \sqrt{T}$ , which we characterize in the following.

Setting  $J = 0$ , the circuit maps to a loop model with two tiles, one associated to  $\mathbb{1}$  (probability  $p$ ) and one to SWAP (probability  $1-p$ ), see Fig. 4(a); the qubits move ballistically under SWAP gates and backscatter under  $\mathbb{1}$ ,

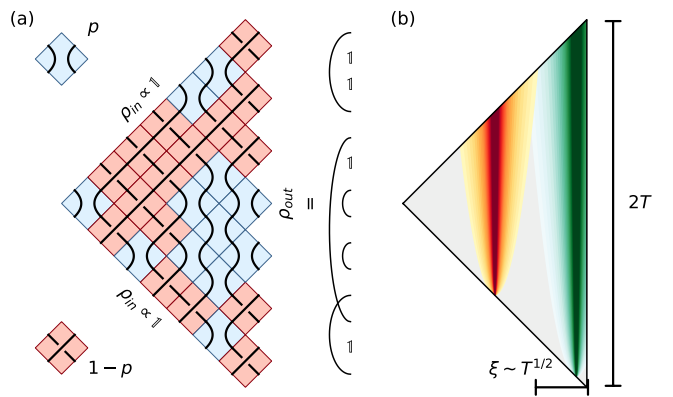


FIG. 4. Critical phase of the non-interacting ( $J = 0$ ) Clifford circuit model. (a) The  $\mathbb{1}$  and SWAP gates (blue and red tiles), randomly arranged in spacetime, define a loop model (a realization for  $T = 7$  is shown). The purification dynamics proceeds left to right; the input qubit worldlines (left) are fully mixed; the output state  $\rho_{\text{out}}$  (right) contains Bell pairs (arcs) and fully mixed qubits ( $\mathbb{1}$  symbols). (b) Coarse-grained view of the purification dynamics ( $T \gg 1$ ). Input qubits a distance  $O(T)$  away from the surface (e.g. orange shaded area) are exponentially unlikely to diffuse to the output state and to contribute entropy. Only qubits within a distance  $\xi \sim T^{1/2}$  (e.g. green shaded area) are likely to contribute entropy.

thus tracing random walks with step size  $\ell$  distributed exponentially,  $\text{Prob}(\ell) \propto (1-p)^\ell$  [62]. Worldlines that begin and end in  $\rho_{\text{out}}$  define a pure Bell pair entirely contained in the system, and thus contribute no entropy; on the contrary, worldlines that begin at the lightcone boundaries ( $\rho_{\text{in}}$ ) and terminate in  $\rho_{\text{out}}$ , or viceversa, yield a fully mixed qubit in the output state and thus contribute one bit of entropy. How many such worldlines are there? Because the qubits undergo diffusion, only those that enter the dynamics within  $O(T^{1/2})$  steps of  $\rho_{\text{out}}$  are likely to contribute entropy, see Fig. 4(b). Thus we have  $S_2(T) \sim \sqrt{T}$ , and a stretched-exponential purification dynamics  $\text{Tr}(\rho_{\text{out}}^2) \sim e^{-c\sqrt{T}}$ , to be compared with the exponential decay in the mixed phase.

*Subsystem purity and quantum code properties.* Having established the existence (and prevalence) of the mixed phase in this class of models, it is interesting to investigate its properties, especially since the nature of the QECC defining the mixed phase remains in general poorly understood [24, 30, 39]. To access such properties in experiment, one needs to measure not only the entropy of the entire state, but also of different subsystems.

First, we consider the combination of Renyi entropies  $I_2^{(\alpha)}(A : \bar{A}) \equiv S_\alpha(A) + S_\alpha(\bar{A}) - S_\alpha(A \cup \bar{A})$  for a bipartition of  $\rho_{\text{out}}$ . For  $\alpha = 1$ , or for any  $\alpha$  in stabilizer states, this would equal the mutual information [63]. We observe that  $I_2^{(2)}(A : \bar{A})$  for any *contiguous*, even-sized bipartition is implicit in the time series  $\{N_+(t) : t = 1, \dots, T\}$  obtained from running the protocol to time  $T$ : indeed,

given a bipartition of the time-like slice where  $\rho_{\text{out}}$  lives,  $A = \{0 \leq \tau < 2t_1\}$ ,  $\bar{A} = \{2t_1 \leq \tau < 2T\}$  for some  $0 < t_1 < T$ , we have

$$I_2^{(2)}(A : \bar{A}) = \log \frac{N_+(T)}{N_+(t_1)N_+(T-t_1)} . \quad (4)$$

Thus running the protocol for  $T$  timesteps yields not just the Renyi-2 entropy of the entire state, but also this combination of Renyi-2 entropies for all (even-sized) contiguous bipartitions, *at no additional cost*.

To access non-contiguous bipartitions, the protocol must be slightly modified. The key idea is “trace out” qubits in the complement of the subsystem of interest,  $\bar{A}$ , by means of depolarization (see [60]). We find that

$$\text{Tr}(\rho_{\text{out},A}^2) = 2^{n_e - n_o} N_+(T; A) / N_{\text{tot}} , \quad (5)$$

where  $n_e$  ( $n_o$ ) is the number of even (odd) qubits in partition  $\bar{A}$ , on which a Bell pair is initialized (measured), and  $N_+(T; A)$  is the number of successful runs based on a modified criterion: the protocol *cannot* fail on any of the  $n_o$  Bell measurements in the partition  $\bar{A}$ ; if a state other than  $|B^+\rangle$  is obtained in such steps, it is reset to  $|B^+\rangle$  and the protocol continues instead of failing [60].

The purity for such non-contiguous bipartitions in stabilizer states can be used to obtain the contiguous code distance  $d_{\text{cont}}$ , an important property of the QECC that protects the mixed phase (see [60]). Numerically, we find that  $\rho_{\text{out}}$  in the mixed phase defines a code with a power-law divergent, subextensive mutual information and contiguous distance (in the bulk), similar to the phenomenology of the mixed phase in other Clifford models [30, 39].

*Discussion.* We have shown that a large class of non-unitary circuits allows direct experimental access to purification dynamics *without postselection*, thus sidestepping a major obstacle toward the observation of entanglement phases in monitored circuits. This is achieved by viewing the (non-unitary) spacetime duals of unitary gates as forced measurements. Our protocol can be used to measure the purity of the whole system as well as arbitrary subsystems, and could enable the experimental investigation of the spatial entanglement structure and QECC properties in the mixed phase of these models.

While the class of models we study is a measure-zero subset of all non-unitary circuits, it is nonetheless very large—in one-to-one correspondence with the space of local unitary circuits. In this Letter we have studied a simple family of models as a demonstration; a thorough exploration of this vast space and of the types of entanglement dynamics it may contain is a fascinating direction for future work.

*Acknowledgments.* We thank Sarang Gopalakrishnan, Michael Gullans, David Huse, Xiaoliang Qi, Tibor Rakovszky and Dominic Williamson for valuable discussions. This work was supported with funding from the Defense Advanced Research Projects Agency (DARPA)

via the DRINQS program (M.I.) and the US Department of Energy, Office of Science, Basic Energy Sciences, under Early Career Award No. DE-SC0021111 (V.K.). The views, opinions and/or findings expressed are those of the authors and should not be interpreted as representing the official views or policies of the Department of Defense or the U.S. Government. M.I. was funded in part by the Gordon and Betty Moore Foundation’s EPiQS Initiative through Grant GBMF4302 and GBMF8686. Numerical simulations were performed on Stanford Research Computing Center’s Sherlock cluster.

---

- [1] Ryszard Horodecki, Paweł Horodecki, Michał Horodecki, and Karol Horodecki, “Quantum entanglement,” *Rev. Mod. Phys.* **81**, 865–942 (2009).
- [2] Luigi Amico, Rosario Fazio, Andreas Osterloh, and Vlatko Vedral, “Entanglement in many-body systems,” *Rev. Mod. Phys.* **80**, 517–576 (2008).
- [3] J. Eisert, M. Cramer, and M. B. Plenio, “Colloquium: Area laws for the entanglement entropy,” *Rev. Mod. Phys.* **82**, 277–306 (2010).
- [4] Pasquale Calabrese and John Cardy, “Entanglement entropy and conformal field theory,” *Journal of Physics A: Mathematical and Theoretical* **42**, 504005 (2009).
- [5] Jens H. Bardarson, Frank Pollmann, and Joel E. Moore, “Unbounded growth of entanglement in models of many-body localization,” *Phys. Rev. Lett.* **109**, 017202 (2012).
- [6] Hyungwon Kim and David A. Huse, “Ballistic spreading of entanglement in a diffusive nonintegrable system,” *Phys. Rev. Lett.* **111**, 127205 (2013).
- [7] Thomas Hartman and Juan Maldacena, “Time evolution of entanglement entropy from black hole interiors,” *Journal of High Energy Physics* **2013**, 14 (2013).
- [8] Hong Liu and S. Josephine Suh, “Entanglement tsunami: Universal scaling in holographic thermalization,” *Phys. Rev. Lett.* **112**, 011601 (2014).
- [9] Márk Mezei and Douglas Stanford, “On entanglement spreading in chaotic systems,” *Journal of High Energy Physics* **2017**, 65 (2017).
- [10] Adam Nahum, Jonathan Ruhman, Sagar Vijay, and Jeongwan Haah, “Quantum entanglement growth under random unitary dynamics,” *Phys. Rev. X* **7**, 031016 (2017).
- [11] C. W. von Keyserlingk, Tibor Rakovszky, Frank Pollmann, and S. L. Sondhi, “Operator hydrodynamics, otocs, and entanglement growth in systems without conservation laws,” *Phys. Rev. X* **8**, 021013 (2018).
- [12] Yichen Huang, “Dynamics of renyi entanglement entropy in local quantum circuits with charge conservation,” arXiv preprint arXiv:1902.00977 (2019).
- [13] Adam R. Brown, Hrant Gharibyan, Stefan Leichenauer, Henry W. Lin, Sepehr Nezami, Grant Salton, Leonard Susskind, Brian Swingle, and Michael Walter, “Quantum Gravity in the Lab: Teleportation by Size and Traversable Wormholes,” arXiv e-prints , arXiv:1911.06314 (2019), arXiv:1911.06314 [quant-ph].
- [14] Rajibul Islam, Ruichao Ma, Philipp M. Preiss, M. Eric Tai, Alexander Lukin, Matthew Rispoli, and Markus Greiner, “Measuring entanglement entropy in a

quantum many-body system,” *Nature* **528**, 77–83 (2015).

[15] Adam M. Kaufman, M. Eric Tai, Alexander Lukin, Matthew Rispoli, Robert Schittko, Philipp M. Preiss, and Markus Greiner, “Quantum thermalization through entanglement in an isolated many-body system,” *Science* **353**, 794–800 (2016).

[16] N. M. Linke, S. Johri, C. Figgatt, K. A. Landsman, A. Y. Matsuura, and C. Monroe, “Measuring the rényi entropy of a two-site fermi-hubbard model on a trapped ion quantum computer,” *Phys. Rev. A* **98**, 052334 (2018).

[17] Tiff Brydges, Andreas Elben, Petar Jurcevic, Benoît Vermersch, Christine Maier, Ben P. Lanyon, Peter Zoller, Rainer Blatt, and Christian F. Roos, “Probing rényi entanglement entropy via randomized measurements,” *Science* **364**, 260–263 (2019), <https://science.scienmag.org/content/364/6437/260.full.pdf>.

[18] Yaodong Li, Xiao Chen, and Matthew P. A. Fisher, “Quantum zeno effect and the many-body entanglement transition,” *Phys. Rev. B* **98**, 205136 (2018).

[19] Brian Skinner, Jonathan Ruhman, and Adam Nahum, “Measurement-induced phase transitions in the dynamics of entanglement,” *Phys. Rev. X* **9**, 031009 (2019).

[20] Yaodong Li, Xiao Chen, and Matthew P. A. Fisher, “Measurement-driven entanglement transition in hybrid quantum circuits,” *Phys. Rev. B* **100**, 134306 (2019).

[21] Soonwon Choi, Yimu Bao, Xiao-Liang Qi, and Ehud Altman, “Quantum error correction in scrambling dynamics and measurement-induced phase transition,” *Phys. Rev. Lett.* **125**, 030505 (2020).

[22] Michael J. Gullans and David A. Huse, “Dynamical purification phase transition induced by quantum measurements,” arXiv e-prints , arXiv:1905.05195 (2019), [arXiv:1905.05195 \[quant-ph\]](https://arxiv.org/abs/1905.05195).

[23] Michael J. Gullans and David A. Huse, “Scalable probes of measurement-induced criticality,” *Phys. Rev. Lett.* **125**, 070606 (2020).

[24] Ruihua Fan, Sagar Vijay, Ashvin Vishwanath, and Yi-Zhuang You, “Self-Organized Error Correction in Random Unitary Circuits with Measurement,” arXiv e-prints , arXiv:2002.12385 (2020), [arXiv:2002.12385 \[cond-mat.stat-mech\]](https://arxiv.org/abs/2002.12385).

[25] Yimu Bao, Soonwon Choi, and Ehud Altman, “Theory of the phase transition in random unitary circuits with measurements,” *Phys. Rev. B* **101**, 104301 (2020).

[26] Chao-Ming Jian, Yi-Zhuang You, Romain Vasseur, and Andreas W. W. Ludwig, “Measurement-induced criticality in random quantum circuits,” *Phys. Rev. B* **101**, 104302 (2020).

[27] Xiangyu Cao, Antoine Tilloy, and Andrea De Luca, “Entanglement in a fermion chain under continuous monitoring,” *SciPost Phys.* **7**, 24 (2019).

[28] Adam Nahum and Brian Skinner, “Entanglement and dynamics of diffusion-annihilation processes with majorana defects,” *Phys. Rev. Research* **2**, 023288 (2020).

[29] Aidan Zabalo, Michael J. Gullans, Justin H. Wilson, Sarang Gopalakrishnan, David A. Huse, and J. H. Pixley, “Critical properties of the measurement-induced transition in random quantum circuits,” *Phys. Rev. B* **101**, 060301 (2020).

[30] Matteo Ippoliti, Michael J. Gullans, Sarang Gopalakrishnan, David A. Huse, and Vedika Khemani, “Entanglement phase transitions in measurement-only dynamics,” arXiv e-prints , arXiv:2004.09560 (2020), [arXiv:2004.09560 \[quant-ph\]](https://arxiv.org/abs/2004.09560).

[31] Ali Lavasani, Yahya Alavirad, and Maissam Barkeshli, “Measurement-induced topological entanglement transitions in symmetric random quantum circuits,” arXiv e-prints , arXiv:2004.07243 (2020), [arXiv:2004.07243 \[quant-ph\]](https://arxiv.org/abs/2004.07243).

[32] Shengqi Sang and Timothy H. Hsieh, “Measurement Protected Quantum Phases,” arXiv e-prints , arXiv:2004.09509 (2020), [arXiv:2004.09509 \[cond-mat.stat-mech\]](https://arxiv.org/abs/2004.09509).

[33] Qicheng Tang and W. Zhu, “Measurement-induced phase transition: A case study in the nonintegrable model by density-matrix renormalization group calculations,” *Phys. Rev. Research* **2**, 013022 (2020).

[34] Javier Lopez-Piqueres, Brayden Ware, and Romain Vasseur, “Mean-field entanglement transitions in random tree tensor networks,” *Phys. Rev. B* **102**, 064202 (2020).

[35] Yaodong Li, Xiao Chen, Andreas W. W. Ludwig, and Matthew P. A. Fisher, “Conformal invariance and quantum non-locality in hybrid quantum circuits,” arXiv e-prints , arXiv:2003.12721 (2020), [arXiv:2003.12721 \[quant-ph\]](https://arxiv.org/abs/2003.12721).

[36] Xhek Turkeshi, Rosario Fazio, and Marcello Dalmonte, “Measurement-induced criticality in (2 + 1)-dimensional hybrid quantum circuits,” *Phys. Rev. B* **102**, 014315 (2020).

[37] Ori Alberton, Michael Buchhold, and Sebastian Diehl, “Trajectory dependent entanglement transition in a free fermion chain – from extended criticality to area law,” arXiv e-prints , arXiv:2005.09722 (2020), [arXiv:2005.09722 \[cond-mat.stat-mech\]](https://arxiv.org/abs/2005.09722).

[38] Sagar Vijay, “Measurement-Driven Phase Transition within a Volume-Law Entangled Phase,” arXiv e-prints , arXiv:2005.03052 (2020), [arXiv:2005.03052 \[quant-ph\]](https://arxiv.org/abs/2005.03052).

[39] Yaodong Li and Matthew P. A. Fisher, “Statistical Mechanics of Quantum Error-Correcting Codes,” arXiv e-prints , arXiv:2007.03822 (2020), [arXiv:2007.03822 \[quant-ph\]](https://arxiv.org/abs/2007.03822).

[40] Lukasz Fidkowski, Jeongwan Haah, and Matthew B. Hastings, “How Dynamical Quantum Memories Forget,” arXiv e-prints , arXiv:2008.10611 (2020), [arXiv:2008.10611 \[quant-ph\]](https://arxiv.org/abs/2008.10611).

[41] Adam Nahum, Sthitadhi Roy, Brian Skinner, and Jonathan Ruhman, “Measurement and entanglement phase transitions in all-to-all quantum circuits, on quantum trees, and in Landau-Ginsburg theory,” arXiv e-prints , arXiv:2009.11311 (2020), [arXiv:2009.11311 \[cond-mat.stat-mech\]](https://arxiv.org/abs/2009.11311).

[42] Jean Dalibard, Yvan Castin, and Klaus Mølmer, “Wavefunction approach to dissipative processes in quantum optics,” *Physical review letters* **68**, 580 (1992).

[43] Paweł Horodecki, “Measuring quantum entanglement without prior state reconstruction,” *Phys. Rev. Lett.* **90**, 167901 (2003).

[44] A. J. Daley, H. Pichler, J. Schachenmayer, and P. Zoller, “Measuring entanglement growth in quench dynamics of bosons in an optical lattice,” *Phys. Rev. Lett.* **109**, 020505 (2012).

[45] Dmitry A. Abanin and Eugene Demler, “Measuring entanglement entropy of a generic many-body system with a quantum switch,” *Phys. Rev. Lett.* **109**, 020504 (2012).

[46] S. J. van Enk and C. W. J. Beenakker, “Measuring  $\text{Tr}\rho^n$  on single copies of  $\rho$  using random measurements,” *Phys. Rev. Lett.* **108**, 110503 (2012).

[47] A. Elben, B. Vermersch, M. Dalmonte, J. I. Cirac, and

P. Zoller, “Rényi entropies from random quenches in atomic hubbard and spin models,” *Phys. Rev. Lett.* **120**, 050406 (2018).

[48] A. Elben, B. Vermersch, C. F. Roos, and P. Zoller, “Statistical correlations between locally randomized measurements: A toolbox for probing entanglement in many-body quantum states,” *Phys. Rev. A* **99**, 052323 (2019).

[49] Andreas Elben, Richard Kueng, Hsin-Yuan Huang, Rick van Bijnen, Christian Kokail, Marcello Dalmonte, Pasquale Calabrese, Barbara Kraus, John Preskill, Peter Zoller, and Benoît Vermersch, “Mixed-state entanglement from local randomized measurements,” arXiv e-prints , arXiv:2007.06305 (2020), [arXiv:2007.06305](https://arxiv.org/abs/2007.06305) [quant-ph].

[50] Bruno Bertini, Pavel Kos, and Tomaž Prosen, “Exact spectral form factor in a minimal model of many-body quantum chaos,” *Phys. Rev. Lett.* **121**, 264101 (2018).

[51] Bruno Bertini, Pavel Kos, and Tomaž Prosen, “Entanglement spreading in a minimal model of maximal many-body quantum chaos,” *Phys. Rev. X* **9**, 021033 (2019).

[52] Bruno Bertini, Pavel Kos, and Tomaž Prosen, “Exact correlation functions for dual-unitary lattice models in  $1+1$  dimensions,” *Phys. Rev. Lett.* **123**, 210601 (2019).

[53] Lorenzo Piroli, Bruno Bertini, J. Ignacio Cirac, and Tomaž Prosen, “Exact dynamics in dual-unitary quantum circuits,” *Phys. Rev. B* **101**, 094304 (2020).

[54] Pieter W. Claeys and Austen Lamacraft, “Maximum velocity quantum circuits,” *Phys. Rev. Research* **2**, 033032 (2020).

[55] Pavel Kos, Bruno Bertini, and Tomaž Prosen, “Correlations in Perturbed Dual-Unitary Circuits: Efficient Path-Integral Formula,” arXiv e-prints , arXiv:2006.07304 (2020), [arXiv:2006.07304](https://arxiv.org/abs/2006.07304) [cond-mat.stat-mech].

[56] M. C. Bañuls, M. B. Hastings, F. Verstraete, and J. I. Cirac, “Matrix product states for dynamical simulation of infinite chains,” *Phys. Rev. Lett.* **102**, 240603 (2009).

[57] M. B. Hastings and R. Mahajan, “Connecting entanglement in time and space: Improving the folding algorithm,” *Phys. Rev. A* **91**, 032306 (2015).

[58] John Napp, Rolando L. La Placa, Alexander M. Dalzell, Fernando G. S. L. Brandao, and Aram W. Harrow, “Efficient classical simulation of random shallow 2D quantum circuits,” arXiv e-prints , arXiv:2001.00021 (2019), [arXiv:2001.00021](https://arxiv.org/abs/2001.00021) [quant-ph].

[59] Michael A. Nielsen and Isaac L. Chuang, *Quantum Computation and Quantum Information: 10th Anniversary Edition*, 10th ed. (Cambridge University Press, USA, 2011).

[60] See online supplemental material for additional details on the spacetime duality transformation, the whole-system and subsystem purity measurement protocols, the state preparation protocol, and the quantum code properties in the mixed phase.

[61] The **iSWAP** gate is defined as  $e^{-i\frac{\pi}{4}(XX+YY)}$ , and is equal to the product of a **SWAP** and a Clifford **ZZ** interaction  $e^{i\frac{\pi}{4}ZZ}$ .

[62] Because the first and second moments of the step size distribution are finite, the behavior of the random walks at long distance and time is the same as for steps of fixed size  $\ell = 1$ .

[63] In general this quantity with  $\alpha = 2$  is not guaranteed to be positive and thus is not a mutual information.

## Supplemental Material: Postselection-free entanglement dynamics via spacetime duality

Matteo Ippoliti and Vedika Khemani  
*Department of Physics, Stanford University, Stanford, CA 94305*

### SPACETIME DUALITY

Here we provide additional details on the notion of *spacetime duality*, where one “rotates” the arrow of time by 90 degrees in spacetime to map a unitary gate  $U$  to a generally different, non-unitary matrix  $\tilde{U}$ .

The duality transformation,  $U_{i_1 i_2}^{o_1 o_2} = \tilde{U}_{i_1 o_1}^{i_2 o_2}$ , rearranges the matrix entries as follows:

$$U = \begin{pmatrix} U_{00}^{00} & U_{00}^{01} & \textcolor{red}{U_{00}^{10}} & \textcolor{red}{U_{00}^{11}} \\ \textcolor{brown}{U_{01}^{00}} & \textcolor{brown}{U_{01}^{01}} & U_{01}^{10} & U_{01}^{11} \\ U_{10}^{00} & U_{10}^{01} & \textcolor{green}{U_{10}^{10}} & \textcolor{green}{U_{10}^{11}} \\ \textcolor{blue}{U_{11}^{00}} & \textcolor{blue}{U_{11}^{01}} & U_{11}^{10} & U_{11}^{11} \end{pmatrix} \implies \tilde{U} = \begin{pmatrix} U_{00}^{00} & U_{00}^{01} & \textcolor{brown}{U_{01}^{00}} & \textcolor{brown}{U_{01}^{01}} \\ \textcolor{red}{U_{00}^{10}} & \textcolor{red}{U_{00}^{11}} & U_{01}^{10} & U_{01}^{11} \\ U_{10}^{00} & U_{10}^{01} & \textcolor{blue}{U_{11}^{00}} & \textcolor{blue}{U_{11}^{01}} \\ \textcolor{green}{U_{10}^{10}} & \textcolor{green}{U_{10}^{11}} & U_{11}^{10} & U_{11}^{11} \end{pmatrix}. \quad (\text{S1})$$

Black entries remain in their place, while two pairs of  $1 \times 2$  blocks (shown in color) are swapped.

In the following we list a few examples.

- $U = \mathbb{1}$ :

$$U = \begin{pmatrix} 1 & 0 & 0 & 0 \\ 0 & 1 & 0 & 0 \\ 0 & 0 & 1 & 0 \\ 0 & 0 & 0 & 1 \end{pmatrix} \implies \tilde{U} = \begin{pmatrix} 1 & 0 & 0 & 1 \\ 0 & 0 & 0 & 0 \\ 0 & 0 & 0 & 0 \\ 1 & 0 & 0 & 1 \end{pmatrix} = \frac{\mathbb{1} + Z_1 Z_1}{2} (\mathbb{1} + X_1 X_2) = 2 |B^+\rangle\langle B^+|, \quad |B^+\rangle = (|00\rangle + |11\rangle)/\sqrt{2}.$$

Thus  $U = \mathbb{1}$  dualizes to a forced Bell measurement, i.e. the projective measurement of  $X_1 X_2$  and  $Z_1 Z_2$  with forced outcomes  $(+1, +1)$ .

- $U = \text{CZ}$  (controlled- $Z$  gate):

$$U = \begin{pmatrix} 1 & 0 & 0 & 0 \\ 0 & 1 & 0 & 0 \\ 0 & 0 & 1 & 0 \\ 0 & 0 & 0 & -1 \end{pmatrix} \implies \begin{pmatrix} 1 & 0 & 0 & 1 \\ 0 & 0 & 0 & 0 \\ 0 & 0 & 0 & 0 \\ 1 & 0 & 0 & -1 \end{pmatrix} = \frac{\mathbb{1} + Z_1 Z_2}{2} (Z_1 + X_1 X_2) = \sqrt{2} \frac{\mathbb{1} + Z_1 Z_2}{2} e^{-i\frac{\pi}{4}Y_1 X_2} Z_1,$$

i.e. the projective measurement of  $Z_1 Z_2$  (with forced outcome  $+1$ ) followed by a specific two-qubit unitary gate.

- $U = \text{SWAP}$ :

$$U = \begin{pmatrix} 1 & 0 & 0 & 0 \\ 0 & 0 & 1 & 0 \\ 0 & 1 & 0 & 0 \\ 0 & 0 & 0 & 1 \end{pmatrix} \implies \tilde{U} = \begin{pmatrix} 1 & 0 & 0 & 0 \\ 0 & 0 & 1 & 0 \\ 0 & 1 & 0 & 0 \\ 0 & 0 & 0 & 1 \end{pmatrix} = U.$$

Thus  $\text{SWAP}$  is a dual-unitary (and self-dual) gate.

These examples illustrate that  $\tilde{U}$  can generally involve a combination of forced measurement and unitary evolution. To characterize this more generally, we can perform a polar decomposition:  $\tilde{U} = V H_0$ , where  $V$  is unitary and  $H_0$  is a positive semidefinite matrix whose eigenvalues are the singular values of  $\tilde{U}$ ,  $H_0 \equiv \sqrt{\tilde{U}^\dagger \tilde{U}}$ . We note that the duality transformation merely reshuffles the matrix entries of  $U$ , hence it cannot change its Frobenius norm:  $\|\tilde{U}\|^2 = \|U\|^2 = \text{Tr}(U^\dagger U) = \text{Tr}(\mathbb{1}) = 4$ . Therefore  $\text{Tr}(H_0^2) = 4$ . Redefining  $H_0 \equiv H_0/2$  we have the identity mentioned in the main text,

$$\tilde{U} = 2VH_0, \quad V \text{ unitary}, \quad H_0 \geq 0, \quad \|H_0\| = 1. \quad (\text{S2})$$

We note that  $H_0$  can be seen as an element of a POVM set [59], completed e.g. by  $H_1 \equiv \sqrt{1 - H_0^2}$ , i.e. another operator  $H_1 \geq 0$  such that  $H_0^2 + H_1^2 = \mathbb{1}$ . The set  $\{H_0, H_1\}$  describes a binary measurement that yields one of two

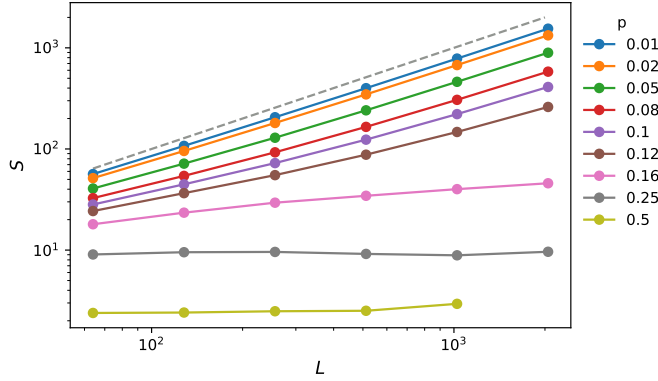


FIG. S1. Numerical simulation of hybrid Clifford circuit model from Ref. [18] with light cone boundary conditions:  $L$  qubits  $-L/2 \leq x < L/2$  evolved for time  $L/2$  with measurements taking place only inside the light cone  $|x| < t$ .  $p$  is the measurement rate;  $p_c = 0.16$  is the known location of the critical point, separating a mixed phase ( $p < p_c$ ) from a pure phase ( $p > p_c$ ). With these boundary conditions, the pure phase has an  $O(1)$ , rather than vanishing, amount of entropy.

possible outcomes,  $\alpha = 0, 1$ , with probabilities  $p_\alpha = \text{Tr}(\rho H_\alpha^2)$ , while the (outcome-averaged) state evolves under a quantum channel  $\rho \mapsto H_0 \rho H_0 + H_1 \rho H_1$ . If  $H_{0,1}$  are orthogonal projectors then this is a projective measurement. More generally, this is a *weak measurement*, achieved e.g. by coupling the system to an ancilla which is then projectively measured. The evolution described by the dualized gate  $\tilde{U}$  is a *forced* weak measurement, since the outcome is deterministically  $\alpha = 0$ .

This gives rise to a generally non-trace-preserving evolution,  $\rho \mapsto 4VH_0\rho H_0V^\dagger$ ; however, the trace increase due to the prefactor and the trace loss due to forcing the  $\alpha = 0$  outcome turn out to exactly compensate each other (with “depolarizing” or “light-cone” boundary conditions, discussed in the following), so that  $\text{Tr } \rho_{\text{out}} \equiv 1$  for hybrid circuits that are spatiotemporally dual to unitary circuits. In particular this proves that the state cannot be annihilated by a forced measurement during the dynamics.

## DETAILS ON PURITY MEASUREMENT PROTOCOL

Here we provide a more detailed derivation of the purity measurement protocol, discuss the effect of “depolarizing boundary conditions”, and how the protocol could be modified to implement conventional open boundary conditions.

### Depolarizing boundary conditions

The protocol we discuss is naturally formulated by starting from a fully mixed state (everywhere except on the central bond  $\mathcal{C}$ ) and tracing out all final qubits (again everywhere except on  $\mathcal{C}$ ). Under the spacetime duality transformation, these initial and final conditions map onto *spatial* boundary conditions of a rather unusual type: the edge qubits are *depolarized* at every time step, i.e. acted upon by a single-qubit fully depolarizing channel  $\Phi(\rho_1) = \text{Tr}(\rho_1) \frac{1}{2}$ , where  $\rho_1$  is a single-qubit density matrix. Thus for the whole state we have  $\rho \mapsto \frac{1}{2} \otimes \text{Tr}_{\{1, \tilde{L}\}}(\rho) \otimes \frac{1}{2}$ . This operation constantly injects some additional entropy into the system through the edges, and one may worry about its effect on the purification dynamics.

We performed numerical simulations of the original Clifford unitary-projective model in Refs. [18, 22], featuring arbitrary gates and projective  $Z$  measurements, starting from a maximally mixed state and depolarizing the edge qubits at every time step. We found that the purification phase diagram is unchanged, see Fig. S1, namely we find that (i) the value of the critical measurement rate  $p_c \simeq 0.16$  is unchanged, (ii) the  $p$ -dependent entropy density in the mixed phase is quantitatively unchanged, and (iii) the only difference is that the pure phase does not achieve zero entropy, but rather a finite,  $p$ -dependent amount of entropy (it still achieves zero entropy density as  $L \rightarrow \infty$ ). This is reasonable, as the entropy constantly injected through the sides is purified in  $O(1)$  time, but not instantly.

Within the class of hybrid circuits that are dual to unitary circuits, the depolarizing boundary conditions described above have a global effect on the circuit. As is clear from viewing the circuit in the unitary direction, all gates that are not in the intersection of the future light cone of the initial Bell state  $|P_C\rangle$  and the past light cone of the final

Bell measurement ( $P_C$ ) (cf. Fig. 2(e) in main text) are elided. Going back to the non-unitary time direction, this amounts to *only allowing measurements inside a light cone*  $|\tilde{x}| < \tilde{t}$ , so that the state outside such light cone remains fully mixed. This places a constraint on the maximum duration of the hybrid time evolution: given a fixed “size”  $\tilde{L} = 2T$  for the output state  $\rho_{\text{out}}$ , measurements (and thus purification) can begin *at most*  $\tilde{T} = T = \tilde{L}/2$  time steps prior. Thus for instance it is not possible to use this approach to probe the very late-time purification dynamics at  $\tilde{T} \gg \tilde{L}$  in the mixed phase [40].

### Normalization

In the main text we show the proportionality between the purity  $\text{Tr}(\rho_{\text{out}}^2|_{2T})$  and the protocol’s success probability  $N_+(T)/N_{\text{tot}}$ , without keeping track of prefactors. Here we show that Eq. (2) in the main text holds as written in two ways: (i) by evaluating both sides on simple circuits, and (ii) by explicitly keeping track of prefactors.

#### Simple circuits

Let us start by taking the simplest example of unitary circuit:  $U_M = \mathbb{1}$ , the brickwork circuit consisting entirely of identity gates. Trivially in this case  $N_+(T) = N_{\text{tot}}$ : a Bell pair projector  $P$  is initialized in  $\mathcal{C}$ , left unperturbed by the  $\mathbb{1}$  gates, and deterministically measured in the following timestep. Conversely, the purification dynamics reduces to the  $p = 1$  model in Fig. 3(b), which is trivially pure:  $\rho_{\text{out}} = P^{\otimes T}$ . Thus the purity is  $1 \forall T$ . By setting both sides equal to 1 in Eq. (2) we recover the (circuit-independent) proportionality factor of 1.

We can additionally consider a dual-unitary circuit  $U_M$ , e.g. one made entirely of SWAP gates. Then  $\rho_{\text{out}} \propto \mathbb{1}$  is maximally mixed,  $\text{Tr}(\rho_{\text{out}}^2) = 2^{-2T}$ . In the unitary time direction, the state at the central bond  $\mathcal{C}$  before each Bell measurement is maximally mixed, and the probability of obtaining  $|B^+\rangle$  is  $1/4$  every time (one out of four equally likely Bell states). Thus  $N_+(T)/N_{\text{tot}} = 4^{-T}$ , again proving that the proportionality factor is 1.

#### Explicit derivation

Here we provide an explicit derivation of the normalizations. Let us define  $\mathcal{D}(T)$  as the value of the tensor network contraction in Fig. 2(e) in the main text for arbitrary  $T$ , without any prefactors. Focusing first on the hybrid time direction, we have  $\text{Tr}(\rho_{\text{out}}^2) = 2^{-4T}\mathcal{D}(T)$ , where we account for the  $2T$  incoming qubits in each copy of  $\rho_{\text{in}}$ , each of which carries a normalizing factor of  $1/2$ . Next we focus on the unitary time direction. Here we have  $2T$  factors of  $1/2$  from the fully mixed input qubits in  $\mathcal{L}$  and  $\mathcal{R}$ ; additionally, each instance of the projector  $P_C$  carries a factor of  $1/2$  (i.e., the horizontal leg contractions at the central bond  $\mathcal{C}$  are equal to  $2P_C$ ). Since there are  $2T$  such projectors at  $\mathcal{C}$  over the course of the protocol ( $T$  initializations and  $T$  measurements), we have overall  $N_+(T)/N_{\text{tot}} = 2^{-4T}\mathcal{D}(T)$ . Thus both sides of Eq. (2) are equal to  $2^{-4T}\mathcal{D}(T)$ , and the proportionality constant is 1.

Here we have glossed over the fact that  $\text{Tr}(\rho_{\text{out}})$  is not trivially guaranteed to be 1, so that one should evaluate the purity as  $\text{Tr}(\rho_{\text{out}}^2)/\text{Tr}(\rho_{\text{out}})^2$ . However it turns out that (despite the non-trace-preserving nature of the dual hybrid circuit  $M$ ) the trace of  $\rho_{\text{out}}$  is in fact 1 under depolarizing or light-cone boundary conditions.

### Open boundary conditions

One could replace the depolarizing boundary conditions with more conventional open boundary conditions (OBCs) at the expense of postselecting on  $L$  Bell measurement outcomes. This can be achieved by having an initial state (in the “laboratory” time direction) made of  $L/2$  nearest-neighbor Bell pairs,  $|B^+\rangle^{\otimes L/2}$ , where  $L$  is now unrelated to the protocol duration  $T$  (i.e. it can be longer or shorter), and projecting onto the same state after  $T$  time steps (which requires postselection).

Viewed in the non-unitary time direction, the Bell-pair dimerization of the initial and final (postselected) states represents hard-wall boundary conditions on the left and right boundaries, see Fig. S2. The initial state of the hybrid dynamics can likewise be chosen to be pure, e.g. by having open boundaries at the edges of the system in the laboratory. This would allow one to simulate *entanglement dynamics* (rather than the purification dynamics we focus on), for arbitrarily long times (as OBCs remove the light-cone constraint and allow arbitrary independent values of  $\tilde{L} \equiv 2T$ ).

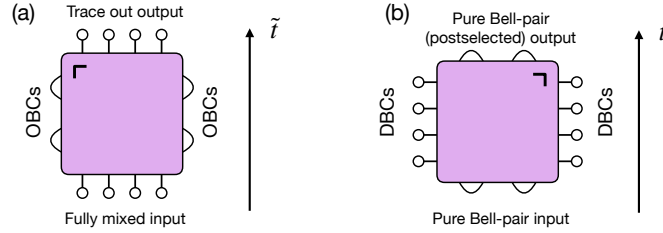


FIG. S2. Transformation of boundary conditions under spacetime duality: sketch for  $L = 4, T = 2$ . (a) A mixed state (bottom) is evolved by a hybrid circuit  $M \otimes M^*$  (pink box) with open boundary conditions (OBCs, left and right arcs). The output is traced out (top). Open circles represent single-qubit  $\mathbb{1}$  operators. (b) Under spacetime duality, the same diagram becomes a unitary circuit  $U_M \otimes U_M^*$  evolving a pure Bell state  $|B^+\rangle^{\otimes 2}$  (arcs at the bottom) with depolarizing boundary conditions (DBCs, left and right) until the state is projected (with postselection) on the Bell state  $|B^+\rangle^{\otimes 2}$  (arcs at the top).

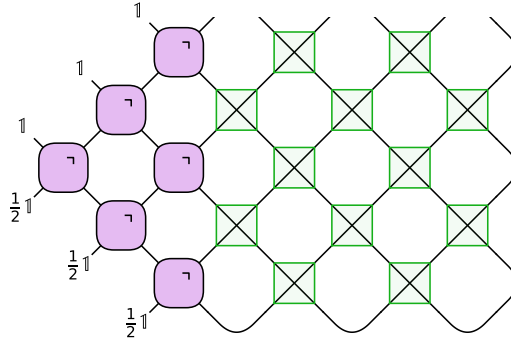


FIG. S3. State preparation protocol. The purple boxes represent doubled gates  $u \otimes u^*$  and all qubit worldlines should be seen as doubled (i.e. as legs of a density matrix). Fully mixed qubit states  $\frac{1}{2}\mathbb{1}$  (bottom left) are evolved by the  $u$  gates and eventually traced out (top left). Ancillae initialized in Bell pair states (bottom right) are evolved with **SWAP** gates (transparent green boxes), with open boundary conditions on the right. As a result, the temporal slice where  $\rho_{\text{out}}$  lives is ‘teleported’ onto a spatial slice in the ancillary system (top right).

and  $\tilde{T} \equiv L/2$ ). The postselection cost scales as  $e^{O(L)}$ . This is exponentially lower than the  $e^{O(LT)}$  postselection cost for conventional simulation of unitary-projective models with finite measurement density in spacetime.

## STATE PREPARATION PROTOCOL

In the main text we have described a method to evaluate the purity of the hybrid circuit output  $\rho_{\text{out}}$  ‘on the fly’, without ever storing the state. However, it may be useful for certain applications to actually prepare the state on a spatial slice of the circuit. Here we describe how to do so with modest overhead ( $O(T)$  ancillas and **SWAP** gates).

The idea is to prepare  $2T$  ancillary qubits on which to store the output state  $\rho_{\text{out}}|_{2T}$ , and to use a version of ‘gate teleportation’ [59] in order to transfer the state from the temporal slice where it is naturally generated onto the ancillas. In practice one needs a chain of  $3T$  qubits: the  $T$  qubits on the left are initialized in a fully mixed state, while the  $2T$  qubits on the right are initialized in nearest-neighbor Bell pairs  $|B^+\rangle^{\otimes T}$ , see Fig. S3. Then the left qubits are evolved via the circuit  $U_M$ , while the right qubits (ancillas) are evolved by a **SWAP** circuit with open boundary conditions on the right wall. As can be seen in Fig. S3, the qubit worldlines are geometrically reflected by the Bell-pair initial condition and by the hard-wall boundary on the right, and thus end up in the correct order on a spatial slice at time  $T$ .

## MEASURING SUBSYSTEM PURITY

Here we discuss how to measure the purity of arbitrary subsystems  $A$  of  $\rho_{\text{out}}$ . To do so, one must obtain the reduced density matrix  $\rho_{\text{out},A} = \text{Tr}_A \rho_{\text{out}}$ . The question is how to perform the partial trace *during the dynamics*,

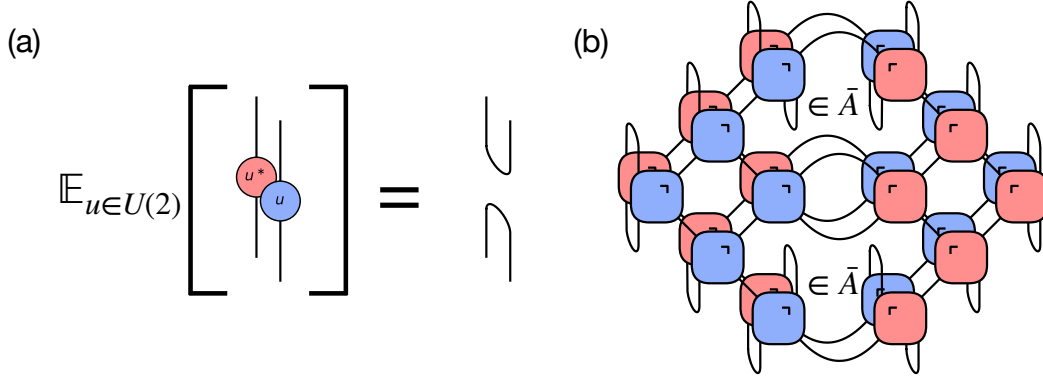


FIG. S4. (a) Depolarizing a qubit by averaging random gates. (b) Protocol for subsystem purity measurement,  $T = 3$  (cf. Fig. 2(d) main text). This represents the purity of subsystem  $A = \{\tilde{0}, \tilde{2}, \tilde{3}, \tilde{5}\}$ , obtained by tracing out the complement  $\bar{A} = \{\tilde{1}, \tilde{4}\}$ .

as  $\rho_{\text{out}}$  exists on a time-like slice of the circuit. One option is to use the state preparation protocol outlined above, repeatedly prepare identical copies of the state, and use a technique based on randomized measurements to obtain the entropy of mixed states [49]. However, this is not necessary: a small modification to the protocol allows measurement of subsystem purities ‘on the fly’, without having to store the two copies of the state.

The key idea is to *depolarize* any qubits that belong to  $\bar{A}$  (and thus need to be traced out) by acting on them with random, uncorrelated single-qubit gates, and to average the results of the protocol over many independent realizations. This uses the property of Haar-random averages,

$$\mathbb{E}_{u \in U(2)}(u\rho u^\dagger) = \text{Tr}(\rho) \frac{\mathbb{1}}{2}. \quad (\text{S3})$$

The Haar average can in fact be simplified to a random Clifford average, by exploiting the 1-design property. The result of averaging many runs of this pure-state dynamics,  $|\psi\rangle \mapsto u|\psi\rangle$ , is to implement a perfect single-qubit depolarizing channel  $\Phi(\rho) \mapsto \text{Tr}(\rho)\mathbb{1}/2$ , see Fig. S4(a). This implements the ‘tracing out’ one needs to compute the reduced density matrix, Fig. S4(b).

More specifically, qubits on the time-like slice where  $\rho_{\text{out}}$  lives play two different roles: there are even qubits,  $\mathcal{E}$ , at time steps where a Bell projector  $P_{\mathcal{C}}$  is initialized, and odd qubits,  $\mathcal{O}$ , at time steps where a Bell projector  $P_{\mathcal{C}}$  is measured, see Fig. S5.

#### Even qubits

Let us consider a qubit  $\tilde{\tau} \in \mathcal{E}$  in  $\rho_{\text{out}}$ , i.e. a time step  $\tau$  where a Bell state  $|B^+\rangle$  has just been created, Fig. S5(b). To depolarize this qubit, one would apply a random Clifford gate on, for example, qubit  $j = -1$  (either one of  $\pm 1 \in \mathcal{C}$  would be equally good) at this time step:

$$\mathbb{E}_u \left[ u_{-1} \otimes \mathbb{1}_1 |B^+\rangle \langle B^+| u_{-1}^\dagger \otimes \mathbb{1}_1 \right] = \frac{\mathbb{1}_{-1}}{2} \otimes \text{Tr}_{-1}(|B^+\rangle \langle B^+|) = \frac{1}{4} \mathbb{1}_{\mathcal{C}}.$$

(The state on the rest of the system outside  $\mathcal{C}$  is omitted.) The outcome of this is a fully mixed state on  $\mathcal{C}$ . The protocol can then continue like in the normal (full-system purity) case. However, there is an extra normalization to take into account: the state  $\mathbb{1}_{\mathcal{C}}$  carries a normalizing factor of  $1/4$  relative to the tensor network diagram  $\mathcal{D}$  it aims to represent. On qubits that belong to  $A$  (and are thus not depolarized), the Bell state  $|B^+\rangle \langle B^+|$  carries only a factor of  $1/2$  relative to the tensor network  $\mathcal{D}$ . These excess factors of  $1/2$ , one for each qubit in  $\mathcal{E} \cap \bar{A}$ , must be compensated by the factor of  $2^{n_e}$  that appears in Eq. (5) in the main text, with  $n_e \equiv |\mathcal{E} \cup \bar{A}|$ .

#### Odd qubits

Next we consider a qubit  $\tilde{\tau} \in \mathcal{O}$  in  $\rho_{\text{out}}$ , i.e. a time step  $\tau$  where a Bell measurement is about to take place, Fig. S5(c). In this case it is sufficient to perform the Bell measurement and ‘reset’ the outcome to  $|B^+\rangle$  regardless

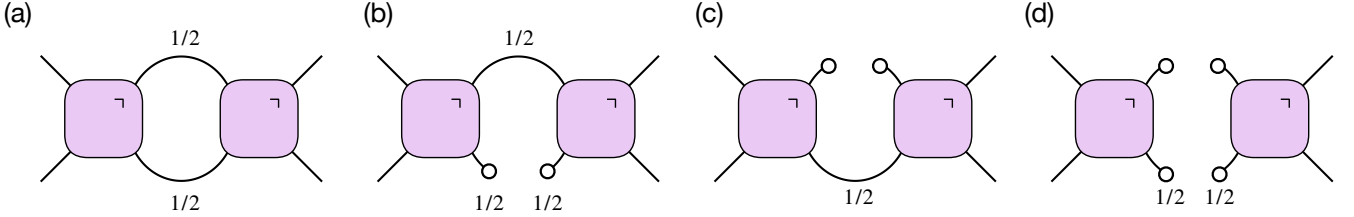


FIG. S5. Accounting of normalizations for subsystem purity calculation at a given timestep. The open circles represent depolarization. (a) No qubits are depolarized. Preparing  $|P\rangle$  and measuring  $\langle P|$  implements the desired diagram up to *two* factors of  $1/2$ . (b) Even qubit is depolarized. Preparing  $\frac{1}{4}|\mathbb{1}\rangle$  and measuring  $\langle P|$  implements the desired diagram up to *three* factors of  $1/2$ —there is an excess factor of  $1/2$  relative to (a). (c) Odd qubit is depolarized. Preparing  $|P\rangle$  and tracing out region  $\mathcal{C}$  implements the desired diagram up to *one* factor of  $1/2$ —there is an excess factor of  $2$  relative to (a). (d) Both the even and the odd qubits are depolarized. Preparing  $\frac{1}{4}|\mathbb{1}\rangle$  and tracing out region  $\mathcal{C}$  implements the desired diagram up to *two* factors of  $1/2$ —the same as in (a). From these cases one obtains the overall normalization  $2^{n_e - n_o}$ .

of the actual outcome. This is done by acting with a single-qubit gate, on e.g. qubit  $j = 1$ , conditioned on the Bell measurement outcome as follows:

$$|B^+\rangle = \frac{|00\rangle + |11\rangle}{\sqrt{2}} \mapsto \mathbb{1}_1; \quad \frac{|00\rangle - |11\rangle}{\sqrt{2}} \mapsto Z_1; \quad \frac{|01\rangle + |10\rangle}{\sqrt{2}} \mapsto X_1; \quad \frac{|01\rangle - |10\rangle}{\sqrt{2}} \mapsto Y_1.$$

Importantly none of the outcomes determines a ‘failure’ – the protocol continues regardless. The process we described corresponds to

$$\rho \mapsto P_{\mathcal{C}} \otimes \text{Tr}_{\mathcal{C}}(\rho)$$

i.e. the preexisting state of qubits  $\pm 1 \in \mathcal{C}$  is simply discarded and replaced by the new state. This process exactly implements the contraction in the tensor network  $\mathcal{D}$ , without normalizations; in comparison, on qubits that belong to  $A$  the state transforms as  $\rho \mapsto P_{\mathcal{C}} \otimes \text{Tr}_{\mathcal{C}}(\rho P_{\mathcal{C}})$  which carries a factor of  $1/2$  relative to the tensor network  $\mathcal{D}$ . The excess factors of  $2$ , one for each qubit in  $\mathcal{O} \cap \bar{A}$ , must be compensated by the factor of  $2^{-n_o}$  that appears in Eq. (5) in the main text, with  $n_e \equiv |\mathcal{E} \cup \bar{A}|$ .

#### Sanity check

We can test the above result’s consistency with the behavior on simple unitary circuits.

Taking  $U_M = \mathbb{1}$  (all-identity circuits), we have  $\rho_{\text{out}} \propto P^{\otimes T}$ , a pure state made of Bell-pair dimers on all even bonds. This state has maximal entanglement entropy  $S_2 = T$  for a non-contiguous bipartition consisting of  $\mathcal{E}$  and  $\mathcal{O}$  (even vs odd qubits), since all  $T$  Bell pairs cross the cut. We can compute this in two ways – setting  $A = \mathcal{E}$  and  $\bar{A} = \mathcal{O}$  or vice versa – and expect the same result as  $\rho_{\text{out}}$  is pure. Let us first take  $A = \mathcal{E}$ . The central bond is sequentially depolarized and measured in the Bell basis. The outcome of each measurement is fully random, with  $1/4$  success probability; thus  $N_+(T; A)/N_{\text{tot}} = 4^{-T}$ . However, because  $n_e = |\bar{A} \cap \mathcal{E}| = T$ , the normalization yields  $\text{Tr} \rho_{\text{out}, A}^2 = 2^T \cdot 4^{-T} = 2^{-T}$ , i.e.  $S_2 = T$ , as expected. Taking  $A = \mathcal{O}$ , we instead have that the central bond is sequentially prepared in the state  $P$  and measured, which trivially always yields the outcome  $|B^+\rangle$ . Thus  $N_+(T; A)/N_{\text{tot}} = 1$  (the protocol can never fail), while the normalization is  $2^{-n_o} = 2^{-T}$ , since  $n_o = |A \cap \mathcal{O}| = T$ . Again, we find  $S_2 = T$  as expected.

## QUANTUM CODE PROPERTIES IN THE MIXED PHASE

Here we report results of numerical simulations of the QECC properties (stabilizer length distribution, mutual information, and contiguous distance) for the Clifford model in the mixed phase,  $0 < p < 1$  and  $J > 0$ .

We start from a fully mixed state on  $\tilde{L}$  qubits ( $\tilde{L}$  even) and evolve it with dual-unitary Clifford gates and two-qubit Bell measurements as described in the main text. A Bell measurement on a pair of qubits  $(\tilde{j}, \tilde{j} + 1)$  is only allowed within a light cone  $|2\tilde{j} + 1 - \tilde{L}| < 2t$ ; the dynamics stops after  $\tilde{T} \equiv \tilde{L}/2$  steps, so that the final time step involves measurements anywhere in the system (‘light cone’ boundary conditions). We put the final stabilizer state in the ‘clipped gauge’ [10, 18], in which the location of stabilizer endpoints carries a precise physical meaning: given two

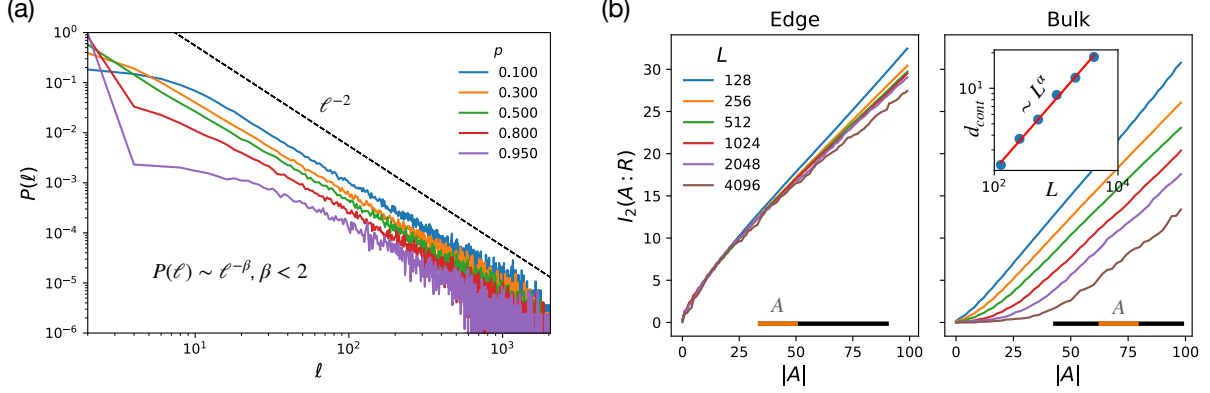


FIG. S6. QECC properties in the mixed phase: numerical results from Clifford simulations of up to  $L = 4096$  qubits with ‘light cone’ boundary conditions. (a) Stabilizer length distribution  $P(\ell)$  for a system of size  $L = 2048$ ,  $J = 1$ , variable  $p$ .  $P(\ell)$  has a power-law tail with exponent  $\beta < 2$ , indicating a power-law, rather than logarithmic, divergence of the mutual information  $I_2(A : \bar{A}) \sim |A|^{2-\beta}$  (we find  $2 - \beta \simeq 0.2$ ). (b) Mutual information  $I_2(A : R)$  between the reference qubits  $R$  and contiguous subsystems  $A$  near the edge (left) and in the bulk (right), for  $J = 0.3$  and  $p = 0.5$ . The development of a plateau  $I_2(A : R) \approx 0$  with increasing system size is associated to a QECC of growing distance. (Inset) Contiguous distance  $d_{\text{cont}}$ , extracted from  $\min\{|A| : I_2(A : R) > 1\}$ , exhibits a power-law divergence.

contiguous regions  $A$  and  $B$ , with  $A$  to the left of  $B$ , the mutual information  $I_2(A : B)$  is equal to the number of stabilizers that start in  $A$  and end in  $B$ . Thus the distribution of stabilizer lengths in the clipped gauge  $P(\ell)$  contains important information about the spatial structure of entanglement in the state. In particular, the mutual information between a contiguous region  $A$  and its complement is approximately proportional to the average stabilizer length  $\bar{\ell} = \int_0^{|A|} d\ell P(\ell) \ell$ . At entanglement critical points this distribution develops a power-law tail  $P(\ell) \sim \ell^{-2}$ , yielding  $I_2(A : \bar{A}) \sim \log |A|$ . This was conjectured to hold into the mixed phase as well (and appears to hold in Haar-random unitary circuits with measurement [24]). However a tail  $P(\ell) \sim \ell^{-\beta}$ ,  $\beta < 2$  has been observed in numerical simulations on Clifford circuits, which translates to a *power-law divergent* mutual information between subsystems,  $I_2(A : \bar{A}) \sim |A|^{2-\beta}$ . Here we find similar behavior, see Fig. S6(b): a power-law tail with exponent seemingly smaller than 2. Numerical fits indicate  $2 - \beta \simeq 0.2$  rather than the value  $\simeq 0.38$  conjectured to be universal for Clifford mixed phases; this could be a genuine difference between the models studied, or could reflect a consequence of boundary conditions or of having evolved the system for shorted times (typically one uses  $T \gtrsim 4L$  while the light-cone boundary conditions impose  $T = L/2$ ).

With the same method one can compute the mutual information between the *reference qubits*  $R$  (i.e. an auxiliary system that purifies the initial fully mixed state) and subsystems  $A$ . This can be obtained entirely from the final mixed state:

$$I_2(A : R) = S(A) + S(R) - S(A \cup R) = S(A) + S(A \cup \bar{A}) - S(\bar{A}) , \quad (\text{S4})$$

which is entirely independent of  $R$ , and we have used the fact that  $A \cup \bar{A} \cup R$  is in a pure state. A region  $A$  such that  $I_2(A : R) \simeq 0$  is one where measurements cannot read-out of the encoded information. In this sense, formation of a QECC (and thus hiding of information in increasingly non-local degrees of freedom) must be accompanied by the emergence of a length scale  $d_{\text{cont}}$  such that  $|A| < d_{\text{cont}} \implies I_2(A : R) \simeq 0$ . We can define the contiguous code distance as  $d_{\text{cont}} = \min\{|A| : I_2(A : R) \geq 1\}$ . Numerical results in Fig. S6(a) show that, for subsystems near the edge, the contiguous distance vanishes – information about  $R$  is immediately gained as qubits are sequentially accessed from the edge. This makes sense, as qubits a distance  $x$  from the edge participate to the dynamics only for  $x$  time steps, and thus do not have time to get strongly entangled with the rest. On the contrary, for regions in the bulk, we see the formation of a plateau in  $I_2(A : R)$  vs  $|A|$  indicative of a power-law divergent contiguous distance,  $d_{\text{cont}} \sim L^\alpha$ . The exponent appears to be  $\alpha \simeq 0.5$ . This exponent, too, was conjectured to take on a universal value  $\sim 0.38$  in the mixed phase. While the values of  $\alpha \simeq 0.5$  and  $2 - \beta \simeq 0.2$  may be individually compatible with 0.38, the fact they deviate in opposite directions is interesting and possibly suggestive of a real difference between the two in these models. Understanding the underlying reason for this discrepancy is an interesting question that we leave for future work.